Aircraft Aerodynamics Wind Tunnel Lab Report

Abstract

This report examines the aerodynamic characteristics of a NACA 0012 aerofoil in a wind tunnel, measuring lift and drag across angles of attack. Using pressure taps and a Pitot rake, data showed a linear lift increase to stall, with low drag at small angles and a sharp rise at higher angles due to flow separation. Tunnel effects were minor at low angles but significant at higher ones. Discrepancies with XFOIL and Thin Airfoil Theory were due to flow separation, viscosity, and tunnel confinement, highlighting the need for corrections and the limits of theoretical models.

1. Introduction

This experiment investigates the aerodynamic properties of a NACA 0012 aerofoil in a wind tunnel, focusing on how surface pressure and wake profiles change with different angles of attack to determine lift and drag. The main objective is to measure surface pressure distribution and profile drag at varying angles, considering factors like wind tunnel effects that may impact accuracy. Using surface pressure taps and Pitot probes, data is collected to calculate lift through pressure integration and drag from the wake's momentum deficit.

2. Methodology

Equipment and Setup

The experiment was conducted using a Plint blower wind tunnel, a low-speed, open-return facility with a 0.457 m x 0.457 m test section. The model tested was a NACA 0012 2D aerofoil, equipped with 23 surface pressure taps (12 on the upper surface, 11 on the lower) for measuring local static pressure. A Pitot rake with 13 probes was used to capture wake profile data downstream of the aerofoil. All data were recorded using LabView software, with measurements taken at varying angles of attack from 0° to 15°.

Experimental Procedure

1. The aerofoil was mounted in the wind tunnel, airflow was stabilized at 20m/s and a reference zero incidence angle at 0 was taken where the pressure from lower and upper surfaces were balanced on the system.
2. Surface pressure readings were taken from the pressure taps at each angle of attack and saved.
3. Wake profile measurements were gathered using the Pitot rake to assess downstream velocity. The rake was adjusted to be centre at the lowest pressure in the wake profile.
4. This process was repeated for angles of attack at 0°, 3°, 6°, 9°, 12°, and 15°. Data was saved 4 times for each angle to mitigate random errors by averaging.

Data Processing

1. **Pressure coefficients** C_p were calculated from static pressure data using:

$$C_p = \frac{p_s - p_\infty}{\frac{1}{2}\rho V_\infty^2} = \frac{p_s - p_\infty}{p_T - p_\infty} \quad \text{(eq1)}$$

Where:

- ρ is the density,
- p_s and p_∞ is the static pressure at i-th taping and freestream static pressure, respectively.
- p_T is the freestream total pressure, v_∞ is the freestream velocity.

2. **Normal Force coefficient** C_n was calculated from pressure coefficient, using:

$$C_n = \frac{1}{c}\int_{Lower} C_p dx - \frac{1}{c}\int_{Upper} C_p dx \quad \text{(eq2)}$$

Where:

- c is the chord length

3. **Lift coefficient** C_l was determined by integrating the surface pressure distribution:

$C_l = C_n \cos(\alpha) - C_a \sin(\alpha)$ (eq3) , Small angle approx. $C_l = C_n \cos(\alpha)$ (eq4

Where:

- C_l is the coefficient of lift

4. **Drag coefficient** C_d was derived from wake velocity data using:

$$C_d = \frac{2}{c}\int_{wake}\left(\frac{u(y)}{V_\infty}\right)\left(1 - \frac{u(y)}{V_\infty}\right)dy \quad \text{(eq5)}$$

$$\frac{u(y)}{V_\infty} = \sqrt{\frac{p_{Tw}(y) - p_{sw}(y)}{p_T - p_\infty}}$$

Where:

- $\frac{u(y)}{V_\infty}$ is the velocity ratio
- $p_{Tw}(y)$ is the total (stagnation) pressure as a function of vertical rake position
- p_∞ and $p_{sw}(y)$ are the freestream static pressures
- p_T is the freestream total pressure

5. **Moment coefficient** C_m For discrete data, the moment about the quarter-chord can be approximated by:

$$C_m = \frac{M}{\frac{1}{2}\rho V_\infty^2} \text{ (eq6)} \quad , \quad M = \sum_{n=i}\left(C_{p,i} \cdot (x_i - 0.25c) \cdot \Delta x_i\right) \text{ (eq7)}$$

Where:

- $C_{p,i}$ is the pressure coefficient at the i-th tap,
- M is the moment about the quarter-chord.
- x_i is the position of the i-th tap along the chord, Δx_i is the spacing between pressure taps.

6. **Blockage corrections** were applied using the total blockage ratio, total blockage effect ϵ:

$$\epsilon = \epsilon_{sb} + \epsilon_{wb} \text{ (eq8)} , \quad \epsilon_{sb} = \frac{K_1 V}{A^{3/2}} , \epsilon_{wb} = \frac{c}{2h} c_{du}$$

Where:

- ϵ_{sb} and ϵ_{wb} are the solid and wake blockage ratios
- A, h are the cross-sectional area and height of test section
- $K_1 = 0.76$, for an aerofoil mounted across the entire width of the test section
- C_{du} uncorrected drag coefficient
- $V = 0.7tcb$ b is the volume of aerofoil model; t, c and b is aerofoil max thickness, chord length, and span respectively

3. Results and Discussion

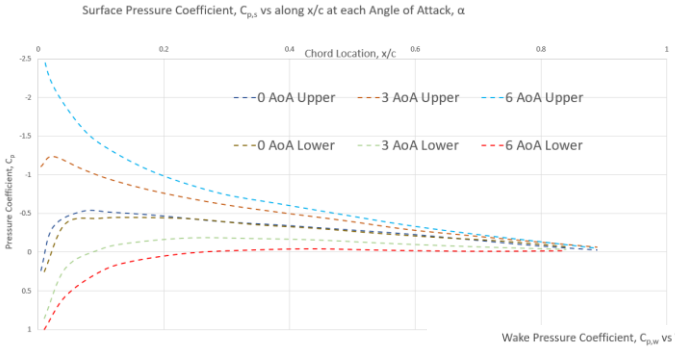

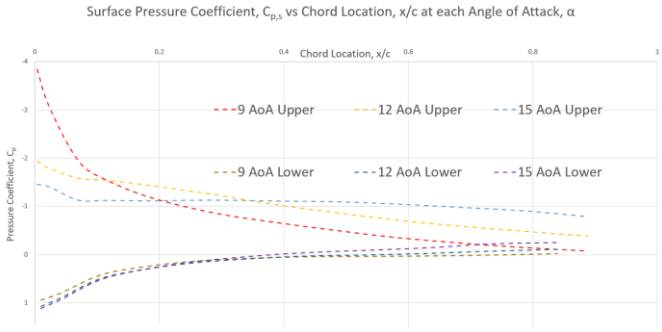

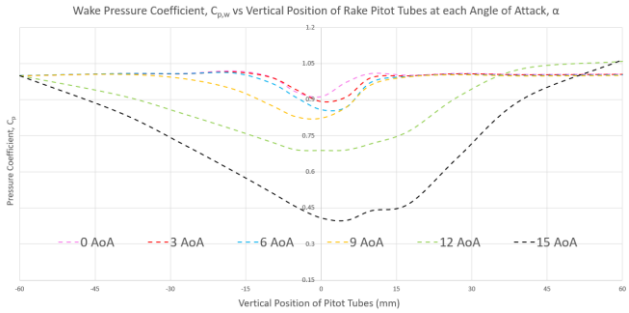

a) Surface pressure coefficients were calculated using freestream total and static pressures measured with a pitot-static tube (P24) and pressure tapings across the aerofoil's mid-span. Results showed a predictable pattern: as the angle of attack (AoA) increased, pressure differences also increased, peaking at 9° AoA and decreasing beyond 12°. Pressure coefficients (Cp) were highest at the leading edge, indicating that lift is primarily generated there, while the lower surface consistently peaked at Cp =1 near the leading edge. The angle of attack (AoA) impacts the pressure gradient and wake behind an aerofoil, affecting lift. At high AoA, boundary layer separation creates a large wake with minimal pressure differences between the upper and lower wake regions. As AoA increases, Cp at the wake center decreases, signalling greater separation and a larger wake, which raises drag. At very high angles, the wake becomes asymmetric and broad, with low Cp values, indicating extensive flow separation, high drag, and potential stall.

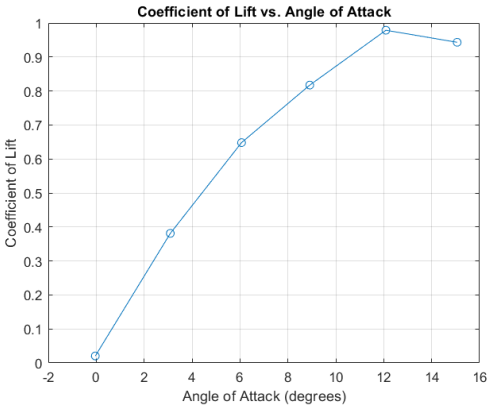

b) From 0° to 10° angle of attack, the coefficient of lift (CoL) rises linearly, as lift is proportional to the angle within this range due to mostly attached flow. At 12°, CoL peaks at about 0.9, marking the critical or stall angle, beyond which lift drops as flow separation begins on the airfoil's upper surface.

c) At low angles of attack (0° to 6°), the drag coefficient remains low and steady, characteristic of laminar flow with attached airflow and low skin friction drag. Here, drag is primarily due to viscous effects, with minimal pressure drag. Around 10°, drag begins to increase as minor flow separation starts on the upper surface, causing a slight rise in pressure drag. Beyond 10°, especially past 12°, drag rises sharply, signaling significant flow separation and the onset of stall.

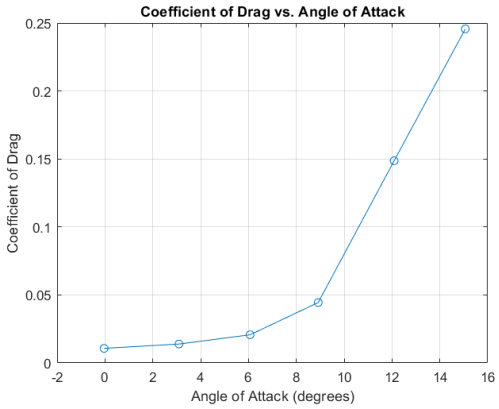

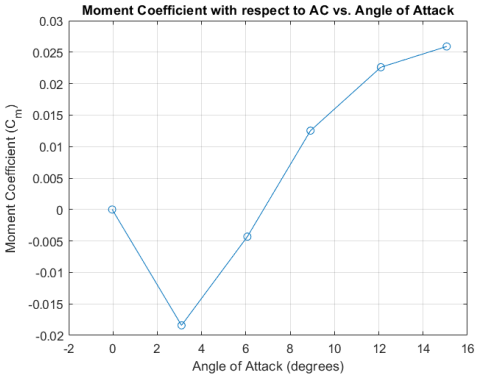

d) The moment coefficient about the quarter chord was calculated using equations 6 and 7. Starting from the leading edge to the trailing.

e) The experimental lift (Cl) and drag (Cd) coefficients differ from Thin Airfoil Theory and XFOIL predictions. Thin Airfoil Theory, which assumes inviscid, incompressible flow, overestimates Cl at higher angles due to its neglect of viscous effects and flow separation. XFOIL, which includes boundary layer effects, provides more accurate Cl predictions but still overestimates lift at higher angles, likely due to limitations in modelling flow separation. Experimental Cl values are consistently lower at high angles as separation reduces lift. For Cd, Thin Airfoil Theory assumes zero drag, while XFOIL accounts for viscosity but underestimates drag compared to experimental results.

EXPERIMENT		AIRFOIL THEORY	XFOIL DATA	
Alpha	C_l	C_l	Alpha	C_l
-0.03659	0.01114	-0.00401	0	0
3.0935	0.38112	0.33924	3	0.449
6.06603	0.6481	0.66521	6	0.691
8.91479	0.81733	0.97762	9	0.924
12.0905	0.9786	1.32587	12	1.016
15.0641	0.9432	1.65196	15	0.685

EXPERIMENT		XFOIL DATA
Alpha	Cd	Cd
-0.03659	0.01071	0.013
3.0935	0.0139	0.0121
6.06603	0.02071	0.0168
8.91479	0.04443	0.0287
12.0905	0.14871	0.0558
15.0641	0.24561	0.1749

Experimental Cd values are higher at all angles, especially beyond 6°, due to flow separation and turbulent wake formation. Further discrepancies likely arise from wind tunnel effects, calibration limits, and sensor variability, reflecting real-world conditions.

f) The glide ratio reveals aerofoil efficiency at different angles of attack. At low angles, the glide ratio increases sharply, peaking around 6°, where lift grows faster than drag. This optimal point, with a glide ratio near 30, represents maximum efficiency (Benson, n.d.)

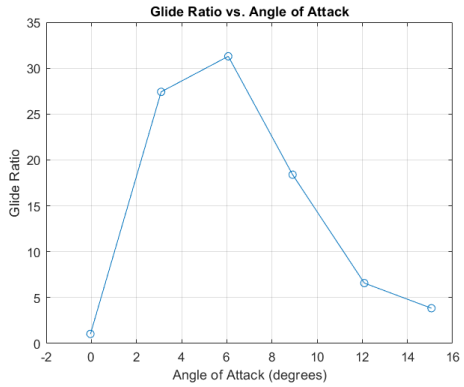

, as airflow remains attached to the aerofoil, keeping drag low and lift high. Beyond 6°, the glide ratio declines due to increased drag from flow separation, which eventually leads to stall. Flow separation occurs when an adverse pressure gradient on the aerofoil's upper surface causes the airflow to slow, detach, and form a turbulent wake, reducing lift and significantly decreasing the glide ratio (Separation of Flow, 2019).

g) Tunnel corrections are needed because wind tunnel walls can constrain airflow around the aerofoil, resulting in measurement deviations from free-flow conditions. This causes effects like solid blockage, where the model restricts airflow and increases velocity, and wake blockage, where the tunnel walls confine the wake, impacting pressure recovery and drag accuracy. Table 1 shows for small angles of attack (0–6 degrees), the total blockage correction values were under 5%, indicating negligible impact. However, as the angle increases beyond 8 degrees, correction values rise, reaching 4.54% at 15 degrees. This suggests that corrections become more significant at higher angles to account for tunnel confinement effects on drag. Nonetheless, since the blockage ratio at 15 degrees remains below 5%, corrections can still be disregarded.

AoA (degrees)	E_sb	E_wb	Blockage (%)
-0.03659	0.010714	0.004646	0.642803
3.093499	0.0139	0.004646	0.695786
6.066029	0.020711	0.004646	0.809058
8.914785	0.044431	0.004646	1.203527
12.09049	0.148707	0.004646	2.937661
15.06411	0.245609	0.004646	4.549156

4. Conclusions

This experiment confirmed the effectiveness of wind tunnel testing for assessing the aerodynamic properties of the NACA 0012 aerofoil. Key findings included a linear lift increase up to stall, a drag rise with angle of attack, and a glide ratio peak at 6°. Experimental results varied from theoretical and XFOIL predictions due to flow separation and wind tunnel effects. Blockage corrections were minor at lower angles but significant at higher angles. Recommendations include using a larger test section to reduce blockage and improving equipment calibration to minimise errors. Overall, the study validated wind tunnel experiments for realistic aerofoil performance evaluation.

References

Benson, T. (n.d.). *L/D Ratio*. [online] www.grc.nasa.gov. Available at: https://www.grc.nasa.gov/www/k-12/VirtualAero/BottleRocket/airplane/ldrat.html.

University, M. (n.d.). *Wind Tunnel Lab Aerofoil Surface Pressure and Profile Drag Measurement*.

Separation of Flow (2019) *Cam.ac.uk*. Available at: http://www-mdp.eng.cam.ac.uk/web/library/enginfo/aerothermal_dvd_only/aero/fprops/introvisc/node9.html